



1 Article

2 Multiple Twisted Chiral Nematic Structures in

3 Cylindrical Confinement

- 4 Milan Ambrožič^{1,2}, Apparao Gudimalla^{3,4}, Charles Rosenblatt⁵, and Samo Kralj^{1,4}
- ¹Department of Physics, Faculty of Natural Sciences and Mathematics, University of Maribor, Koroška 160,
- 6 2000 Maribor, Slovenia
- ²Faculty of Industrial Engineering, Šegova 112, Novo mesto, Slovenia
- 8 ³Jožef Stefan International Postgraduate School, Jamova 39, 1000 Ljubljana, Slovenia
- 9 ⁴Condensed Matter Physics, Jožef Stefan Institute, Jamova 39, 1000 Ljubljana, Slovenia
- 10 Department of Physics, Case Western Reserve University Cleveland, Ohio 44106, USA

Abstract: We study theoretically and numerically chirality and saddle-splay elastic constant (K_{24}) enabled stability of multiple-twist-like nematic liquid crystal (LC) structures in cylindrical confinement. We focus on the so-called radially-z-twisted (RZT) and radially-twisted (RT) configurations, which simultaneously exhibit twists in different spatial directions. We express free energies of the structures in terms of dimensionless wave vectors, which characterise the structures and play the role of order parameters. The impact of different confinement anchoring conditions is explored. A simple Landau-type analysis provides insight into how different model parameters influence the stability of structures. We determine conditions for which the structures are stable in chiral and also nonchiral LCs. In particular, we find that the RZT structure could exhibit macroscopic chirality inversion on varying the relevant parameters. This phenomenon could be exploited for measurements of K_{24} .

Keywords: liquid crystals; chirality; saddle-splay elasticity; double twist deformations

1. Introduction

Chirality is pervasive in nature and refers to cases where an object and its mirror image are different [1–3]. It signals the absence of inversion symmetry, giving rise to right-handed and left-handed appearance and behaviour. Chirality is present throughout physics and often impacts or even dominates numerous important natural phenomena. For example, chiral symmetry plays an important role in the Standard Model of physics [4]. Functionalities of several essential components of biological cells rely heavily on chirality [3]. Furthermore, it could be exploited in various technological and medical applications [5,6,7]. By exploiting chirality one could engineer new materials with extraordinary properties (e.g., metamaterials exhibiting negative refractive index [8]). Therefore, a deep understanding of chirality and related emergent behaviours are of interest throughout the physical and biological sciences.

However, several issues related to chirality remain unresolved even at a fundamental level. For instance, the molecular origins of chirality and the relative role of chiral symmetry breaking remain an open problem [9]. In particular, mechanisms involved in the transfer of chirality from microscopic to macroscopic level [10] are not sufficiently understood. A convenient system with which to gain a deeper understanding of the latter feature are chiral uniaxial nematic liquid crystals (NLCs; a list of abbreviations appears at the end), one of the simplest representatives of anisotropic soft materials [11,12]. These systems are relatively easily accessible experimentally, structural changes can be triggered by relatively weak external stimuli, and a macroscopic chiral response can be achieved using different pathways.

Uniaxial NLCs consist of approximately rod-shaped objects that in bulk equilibrium exhibit long-range orientational order and the absence of translational order [11]. The local orientational

order is commonly described by the mesoscopic nematic director field \vec{n} , exhibiting head-to-tail invariance – the states $\pm \vec{n}$ are physically equivalent. In the classical Oseen-Frank approach [11] the elastic free energy is expressed as the sum of the so-called splay, twist, bend, and saddle-splay contributions, weighted by Frank splay (K_{11}), twist (K_{22}), bend (K_{33}), and saddle-splay (K_{24}) elastic constants. These contributions penalize different elastic distortions and determine equilibrium nematic director field patterns.

In the bulk achiral nematic phase \vec{n} is spatially homogeneously aligned along a single symmetry breaking direction. In a simple chiral nematic (also referred to as the cholesteric) phase, in the bulk equilibrium structure \vec{n} twists in space describing a helix, where \vec{n} is always perpendicular to the helix axis. This structure exhibits only a single twist (i.e., it twists only along one spatial direction) deformation.

Even more complex structures could be formed in chiral materials exhibiting propensity for saddle-splay deformations [13,14], which in LCs is controlled by the saddle splay elastic constant K_{24} . The energy elastic term weighted by K_{24} equals the Gaussian curvature of a hypothetical local surface [11], whose surface normal is determined by \vec{n} . This term is different from zero for the nematic structures displaying, e.g., double twist like deformations, in which is \vec{n} varying in two orthogonal directions. Consequently, such structures could decrease the overall free energy for a large enough value of K_{24} . Note that the saddle-splay elastic term can be expressed as pure divergence, and can be mathematically integrated out to the surface confining the LC. Therefore, it affects LC order through boundary conditions. In most cases the saddle-splay enforced boundary tendency is masked by stronger surface anchoring conditions. For this reason, the K_{24} contribution is often ignored in theoretical modelling [11,14]. Its magnitude range is determined by Ericksen's inequality [15] $0 < K_{24} < K_{1,2}^{(min)}$, where $K_{1,2}^{(min)}$ corresponds to the lower elastic modulus of the twist (K_{22}) and splay (K_{11}) elastic deformations. Furthermore, due to the anchoring strength "masking" effect it is relatively difficult to measure the magnitude of K_{24} . Namely, for strong enough anchoring [11] (i.e. RW/K>>1, where R is the characteristic confinement length, K stands for the average Frank elastic constant, and W is the surface anchoring strength coefficient), the surface anchoring contribution overrides the competing K_{24} contribution in the relevant surface Euler-Lagrange equilibrium equations. Consequently, only a few experimental measurements of K_{24} are reported [16,17,18]. Several of these measurements report values of K_{24} that are close to $K_{1,2}^{(min)}$.

We note that a natural decomposition of representative nematic elastic distortions was recently proposed by Selinger [19]. Four bulk elastic normal modes were introduced representing distinct irreducible representations of the rotational symmetry group, characterising NLC symmetry. These are referred to as the *double splay*, *double twist*, *bend*, and *biaxial splay* mode, which could be separately and independently excited. On the contrary, the classical (single) splay, (single) twist, bend, and saddle-splay distortions [11,19] are, in general, coupled. Namely, the saddle-splay term can be expressed as a sum of *double splay*, *double twist*, and *biaxial splay* mode.

Nematic structures exhibiting nonplanar 3D nematic distortions (e.g., double twist deformations) impose elastic frustrations, which can be in bulk resolved by introducing assemblies of topological defects [20,21], as manifested in Blue Phases (BPs) [22,23,24]. In NLCs, description of defects would require more complex structural description in terms of the tensor nematic order parameter [11], which allows local melting of LC order and presence of biaxial states [25]. On the other hand, such deformation could be realized without defects in appropriate confinement geometries, where most often cylindrical confinements [26,27,28,29,30,31] are used. Note that stable 3D realisations of topological defects are of interest for science in general. For instance, if physical fields represent fundamental entities of nature [32], than topological defects might represent [33] fundamental particles in the conventional "particle"-based natural description.

In this contribution, we consider nematic structures in chiral LCs in cylindrical confinement. We focus on (meta) stability of multiple-twist-type structures, which exhibit variations of the nematic molecular field simultaneously in at least two orthogonal spatial directions. We show that several structural properties can arise in the context of a simple Landau-type model. A more general analysis is carried out numerically. We determine regimes where one could observe a change in the

handedness of structures by varying relevant material parameters. Furthermore, we determine regimes in which the saddle-splay elasticity sensitively controls the stability of competing structures.

100 **2. Results**

101

102

103

104

105

106

126

127

128

129

130

131

132

133

134

135

136

137

138

Of our interest are defect-free spontaneously twisted NLC structures within an infinitely long cylinder of radius R. For this reason, we use cylindrical coordinates $\{r, \varphi, z\}$, defined by the unit vector triad $\{\vec{e}_r, \vec{e}_\varphi, \vec{e}_z\}$. We consider two different ansatzes, which approximate well two qualitatively different families of solutions that are expected to be stable for geometries and boundary conditions of our interest [26,27].

The first class is represented by [26,27]

$$\vec{n}^{(i)} = \cos\psi \sin\Omega \ \vec{e}_r + \sin\psi \sin\Omega \ \vec{e}_{\varphi} + \cos\Omega \ \vec{e}_z, \tag{1a}$$

108
$$\psi = q_1 z - \varphi, \quad \Omega = \frac{\pi}{2} - q_2 r \quad sin\psi, \tag{1b}$$

- where the wave vectors q_1 and q_2 are variational parameters. A typical representative structure is shown in **Figure 1a** and in the Supplementary material.
- In the Cartesian coordinates $\{x, y, z\}$ the ansatz reads
- 112 $\vec{n}^{(i)} = \cos(q_1 z) \sin\Omega \vec{e}_x + \sin(q_1 z) \sin\Omega \vec{e}_y + \cos\Omega \vec{e}_z$
- 113 Cases $q_1 \neq 0$ and $q_2 \neq 0$ determine multiple-twisted solutions. In these patterns, to which we refer to as *radially–z–twisted* (RZT) structures, twist deformation is realized both along the \vec{e}_r and \vec{e}_z directions [26]. This ansatz also encompasses single twisted structures. For example, for $q_2 = 0$ a structure twisting around the z axis is expressed as

117
$$\vec{n}^{(i)} = \cos(q_1 z - \varphi) \quad \vec{e}_r + \sin(q_1 z - \varphi) \quad \vec{e}_{\varphi}, \tag{2}$$

- Which corresponds to a classical cholesteric solution with wave vector q_1 .
- The second family of solution corresponds to the *radially-twisted* (RT) structures [26,27], where the twist is realised along \vec{e}_r , see **Figure 1b**. For this purpose, we use the ansatz

$$\vec{n}^{(ii)} = \sin\alpha \ \vec{e}_{\omega} + \cos\alpha \ \vec{e}_{z}. \tag{3a}$$

Here $\alpha = \alpha(r)$ and to avoid a singularity at the cylinder axis we impose the condition $\alpha(0) = 0$. Previous numerical studies [26,31] have revealed that the dependence of $\alpha(r)$ is roughly linear in r, even for large twists of \bar{n} . Consequently, we use the approximation

$$\alpha = q_{RT}r. \tag{3b}$$

These structures were numerically studied in Refs. 26,27, and 31, where their stability was analysed. Our proposed ansatzes well mimic numerically obtained structures for anchoring conditions of our interest for relatively small wave vectors and in the approximation of equal Frank elastic constants $K_{11} = K_{22} = K_{33}$. In the cases examined, the free energies of structures obtained i) numerically by solving relevant Euler Lagrange equations or ii) using our ansatzes differ by less than 10%. By using the analytical ansatzes, we were able to carry out a Landau-type approach, which enabled a more detailed insight into the stability of structures of interest on varying different material dependent parameters.

In the following we use the approximation of equal elastic constants $K \equiv K_{11} = K_{22} = K_{33}$, but allow $K_{24} \neq K$. At the cylinder's lateral wall, r = R, we impose for the positive anchoring strength W>0 (see Eq.(19) in Methods) either a) homeotropic anchoring $(\vec{e} = \vec{e}_r)$, b) tangential anchoring along \vec{e}_z (i.e., $(\vec{e} = \vec{e}_z)$, or c) tangential anchoring along $\vec{e}_{\varphi}(\vec{e} = \vec{e}_{\varphi})$. We henceforth refer to these cases as a) *homeotropic*, b) *zenithal tangential*), and c) *azimuthal tangential* anchoring, respectively. For

W < 0 these cases correspond to isotropic tangential anchoring in a plane with the surface normal in the direction \vec{e} . Note that in our study the latter case in sensible only for the condition (a).

For later convenience we introduce the following dimensionless quantities: Q = qR, $Q_1 = q_1R$, $Q_2 = q_2R$, $Q_{RT} = q_{RT}R$, $k_{24} = K_{24}/K$, w = RW/K, and the dimensionless free energy is scaled in units of $F_0 = \pi KH$. Therefore $F \to F/F_0$, where H is the height of cylinder. For numerical convenience, we suppose that H is either large in comparison with the period $p = 2\pi/q_1$, or an integer number of p.

145 2.1. Free energies of structures

141

142

143

144

146

147 148 149 Using the ansatzes Eq. (1) and Eq. (3) and the scaling described above, we calculate free energies F of the structures (see Eq. (1)). For later convenience the energies are decomposed as $F^{(i)} = F_e^{(i)} + F_s^{(i)}$ and $F^{(ii)} = F_e^{(ii)} + F_s^{(ii)}$ for the first (RZT) and second class (RT) of solutions, respectively.

We consider first the family of solutions labelled by $\vec{n}^{(i)}$ (Eq. (1)). The elastic contribution is

$$F_e^{(i)} = \frac{(Q - Q_2)^2}{2} + \frac{Q_1^2 Q_2^2}{8} + \frac{Q_1}{2} \left(\frac{Q_1}{2} + (1 - k_{24})Q_2 - Q\right) \left(1 + \frac{I_1(2Q_2)}{Q_2}\right) \tag{4}$$

Now let $F_s^{(i)}$ stand for the interface contribution, which is different for a) homeotropic ($F_s^{(i)} = 152$ $F_{s,h}^{(i)}$), b) zenithal ($F_s^{(i)} = F_{s,z}^{(i)}$), and c) azimuthal $F_s^{(i)} = F_{s,\phi}^{(i)}$ anchoring:

153
$$F_{s,h}^{(i)} = \frac{3w}{4} - \frac{w}{4} \frac{J_1(2Q_2)}{Q_2}, \tag{5a}$$

154
$$F_{s,z}^{(i)} = \frac{w}{2} - \frac{w}{2} J_0(2Q_2), \tag{5b}$$

155
$$F_{s,\varphi}^{(i)} = \frac{3w}{4} + w \left(\frac{J_1(2Q_2)}{4Q_2} - \frac{J_0(2Q_2)}{2} \right).$$
 (5c)

- Here J_0 and J_1 stand for the Bessel functions of order 0 and 1, respectively.
- The second class of solutions is determined by the elastic term

158
$$F_e^{(ii)} = \frac{1}{2}(Q + Q_{RT})^2 + \left(1 - k_{24} + \frac{Q}{Q_{RT}}\right)\sin^2 Q_{RT} + \int_0^1 \frac{\sin^2(Q_{RT}x)}{x} dx, \tag{6}$$

and surface contributions

160
$$F_{s,h}^{(ii)} = w,$$
 (7a)

161
$$F_{s,z}^{(ii)} = w \sin^2 Q_{RT}, \tag{7b}$$

162
$$F_{s,\varphi}^{(ii)} = w \cos^2 Q_{RT}. \tag{7c}$$

We obtain solutions by varying the variational parameters Q_1 , Q_2 and Q_{RT} for given material properties (determined by Q, k_{24} , w) and boundary conditions.

Of interest is the determination of regimes where radially–z–twisted (RZT) or radially-twisted (RT) structures are stable. We first perform an analytic analysis of structures where we expand the free energies in the limit of relatively small dimensionless wave numbers Q_1 , Q_2 and Q_{RT} . Then we shall perform a more detailed stability analysis numerically.

169 2.2. Landau-type analysis

165

166

167

168

We first consider RZT (class 1) structures using the ansatz Eq. (4). By minimizing the total free energy $F^{(i)}$ with respect to Q_1 it follows that

172
$$Q_1 = \frac{Q + (k_{24} - 1)Q_2}{1 + \frac{Q_2^2}{2(1 + \frac{J_1(2Q_2)}{Q_2})}}.$$
 (8)

In the following we examine regimes only of relatively low wave vectors Q_2 (i.e. $Q_2 \ll 1$), for which Eq. (8) yields

175
$$Q_1 \sim Q + (k_{24} - 1)Q_2 - \frac{Q_2^2 Q}{4}. \tag{9}$$

Taking this into account, we expand $F^{(i)}$ up to the fourth power in Q_2 . It follows that

$$177 \qquad F_h^{(i)} = \frac{w}{2} + \frac{(Q - Q_2)^2}{2} - k_{24} Q Q_2 + \frac{8k_{24} - 4k_{24}^2 + 2Q^2 + w}{8} Q_2^2 + \frac{Q(k_{24} - 1)}{2} Q_2^3 \\ + \frac{24 - 48k_{24} + 24k_{24}^2 - 5Q^2 - 2w}{96} Q_2^4, \quad (10a)$$

$$178 \qquad F_z^{(i)} = \frac{(Q-Q_2)^2}{2} - k_{24}QQ_2 + \frac{4k_{24} - 2k_{24}^2 + Q^2 + 2w}{4}Q_2^2 + \frac{Q(k_{24} - 1)}{2}Q_2^3 + \frac{24 - 48k_{24} + 24k_{24}^2 - 5Q^2 - 12w}{96}Q_2^4, \tag{10b}$$

179
$$F_{\varphi}^{(i)} = \frac{w}{2} + \frac{(Q - Q_2)^2}{2} - k_{24}QQ_2 + \frac{8k_{24} - 4k_{24}^2 + 3w}{8}Q_2^2 + \frac{Q(k_{24} - 1)}{2}Q_2^3 + \frac{24 - 48k_{24} + 24k_{24}^2 - 10w}{96}Q_2^4.$$
 (10c)

- Here $F_h^{(i)}$, $F_z^{(i)}$, and $F_{\varphi}^{(i)}$ denote $F^{(i)}$ for homeotropic, zenithal, and azimuthal anchoring,
- 181 respectively. We thus obtain a Landau-type expansion of the form $F^{(i)} = F_0^{(i)} + \alpha_1 Q_2 + \alpha_2 Q_2^2 + \alpha_3 Q_2^2 +$
- 182 $\alpha_3 Q_2^3 + \alpha_4 Q_2^4$ where Q_2 and $\{\alpha_1, \alpha_2, \alpha_3, \alpha_4\}$ play the role of order parameter and Landau expansion
- 183 coefficients, respectively.
- For achiral LCs (Q = 0) one obtains

$$F_h^{(i)} = \frac{w}{2} + \frac{8k_{24} - 4k_{24}^2 + w + 4}{8} Q_2^2 + \frac{24 - 48k_{24} + 24k_{24}^2 - 2w}{96} Q_2^4, \tag{11a}$$

$$F_z^{(i)} = \frac{4k_{24} - 2k_{24}^2 + 2w + 4}{4}Q_2^2 + \frac{24 - 48k_{24} + 24k_{24}^2 - 12w}{96}Q_2^4, \tag{11b}$$

$$F_{\varphi}^{(i)} = \frac{w}{2} + \frac{8k_{24} - 4k_{24}^2 + 3w + 4}{8}Q_2^2 + \frac{24 - 48k_{24} + 24k_{24}^2 - 10w}{96}Q_2^4. \tag{11c}$$

The spatially homogeneous order becomes unstable with respect to the RZT class of solutions where the coefficients α_2 that weight the Q_2^2 contribution in Eq. (11) change sign. From the condition $\alpha_2 = 0$ one could deduce a critical value k_{24} above which the RZT structures become stable:

$$k_{24}^{(h)} = 1 + \sqrt{1 + \frac{w}{4}},\tag{12a}$$

193
$$k_{24}^{(z)} = 1 + \sqrt{1+w},$$
 (12b)

$$k_{24}^{(\varphi)} = 1 + \sqrt{1 + \frac{3w}{4}}. (12c)$$

197 198 199

200

205

206

207

208

Here $k_{24}^{(h)}$, $k_{24}^{(z)}$, and $k_{24}^{(\phi)}$ determine the critical values of k_{24} for homeotropic, zenithal, and azimuthal anchoring, respectively. Note that in the approximation of equal elastic constants the Ericksen's critical value of K_{24} is given by $k_{24}^{(e)} = 2$. Therefore, in the absence of chirality K_{24} could trigger twisted structures only for w < 0, which in our modelling is physically meaningful for the case given by Eq. (12a).

Next, we focus on the RT structures using the ansatz of Eq. (3). When $Q_{RT} \ll 1$ it follows

$$F_e^{(ii)} \sim \frac{Q^2}{2} + 2QQ_{RT} + (2 - k_{24})Q_{RT}^2 - \frac{QQ_{RT}^3}{3} + \frac{\left(k_{24} - \frac{5}{4}\right)}{3}Q_{RT}^4.$$
 (13)

It is easy to estimate the equilibrium value of the chirality wave number Q_{RT} of the RT structure if both Q and Q_{RT} are small. We use Eq. (13) and Eq. (7) and free energy minimization yields

$$Q_{RT} = -Q/(2 + \Delta - k_{24}), \tag{14}$$

with $\Delta = 0$ for homeotropic anchoring, and $\Delta = \pm w$ for tangential anchorings (positive sign for zenithal anchoring and negative sign for azimuthal anchoring). Note the Eq. (14) is valid only in the limit when $|Q_{RT}| < 1$.

For achiral LCs it follows

209
$$F_h^{(ii)} \sim w + (2 - k_{24})Q_{RT}^2 + \frac{(k_{24} - \frac{5}{4})}{3}Q_{RT}^4.$$
 (15a)

210
$$F_z^{(ii)} \sim (2 - k_{24} + w)Q_{RT}^2 + \frac{(k_{24} - \frac{5}{4} - w)}{3}Q_{RT}^4.$$
 (15b)

211
$$F_{\varphi}^{(ii)} \sim w + (2 - k_{24} - W)Q_{RT}^2 + \frac{(k_{24} - \frac{5}{4} + w)}{2}Q_{RT}^4.$$
 (15c)

The critical conditions read

$$k_{24}^{(h)} = 2, (16a)$$

$$k_{24}^{(z)} = 2 + w, (16b)$$

$$k_{24}^{(\varphi)} = 2 - w. ag{16c}$$

Therefore, in achiral LCs the saddle splay elasticity may trigger the RT structure below $k_{24}^{(e)} = 2$ only for the case of azimuthal anchoring.

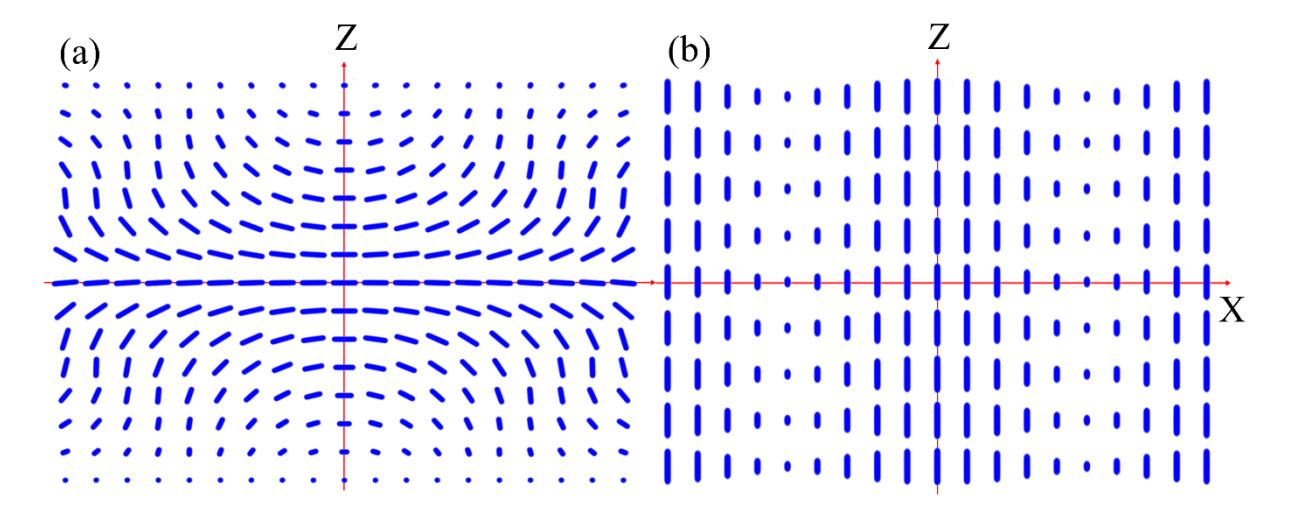


Figure 1. Twisted nematic structures. (a) The radially-z-twist deformation. $Q_1 = 1.0$, $Q_2 = 1.0$. Twist is realised both along the \vec{e}_{φ} and \vec{e}_z directions. (b) The radially-twisted structure. Here, the twist is realised along \vec{e}_T . $Q_{RT} = 1.1$.

2.3. Numerical analysis

We next explore the (meta) stability of double-twist structures in chiral LCs. Of particular interest is the determination of regimes in which the reversal of macroscopic chirality could be realised by varying a relevant parameter. Note that our estimates work well for dimensionless wave vectors less than one. Most of the "interesting" phenomena are realized in this regime. Therefore, results obtained for wave vectors larger than one are only indicative.

2.3.1. RZT structure: homeotropic anchoring

We focus first on RZT (class 1) structures and homeotropic anchoring. Of interest is the exploration of the impact of the saddle–splay constant k_{24} and intrinsic chirality Q for relatively weak anchoring, for which we set to w = 1. In **Figure 2** we plot Q_1 and Q_2 equilibrium values (i.e., they determine local minima in F) on varying Q between 0 and 1. For the case Q = 0 (achiral nematic) the RZT structures could be triggered only in the regime $k_{24} > k_{24}^{(e)} \equiv 2$. However, for chiral LCs, k_{24} efficiently promotes the stability of RZT structures well below $k_{24}^{(e)}$. Furthermore, for $k_{24} = 0$, it holds that $Q_2 = 0$ and $Q_1 = Q$. This solution corresponds to the classic cholesteric structure, see Eq. (2). Graphs in **Figure 2** also reveal that a value of k_{24} can be extracted experimentally.

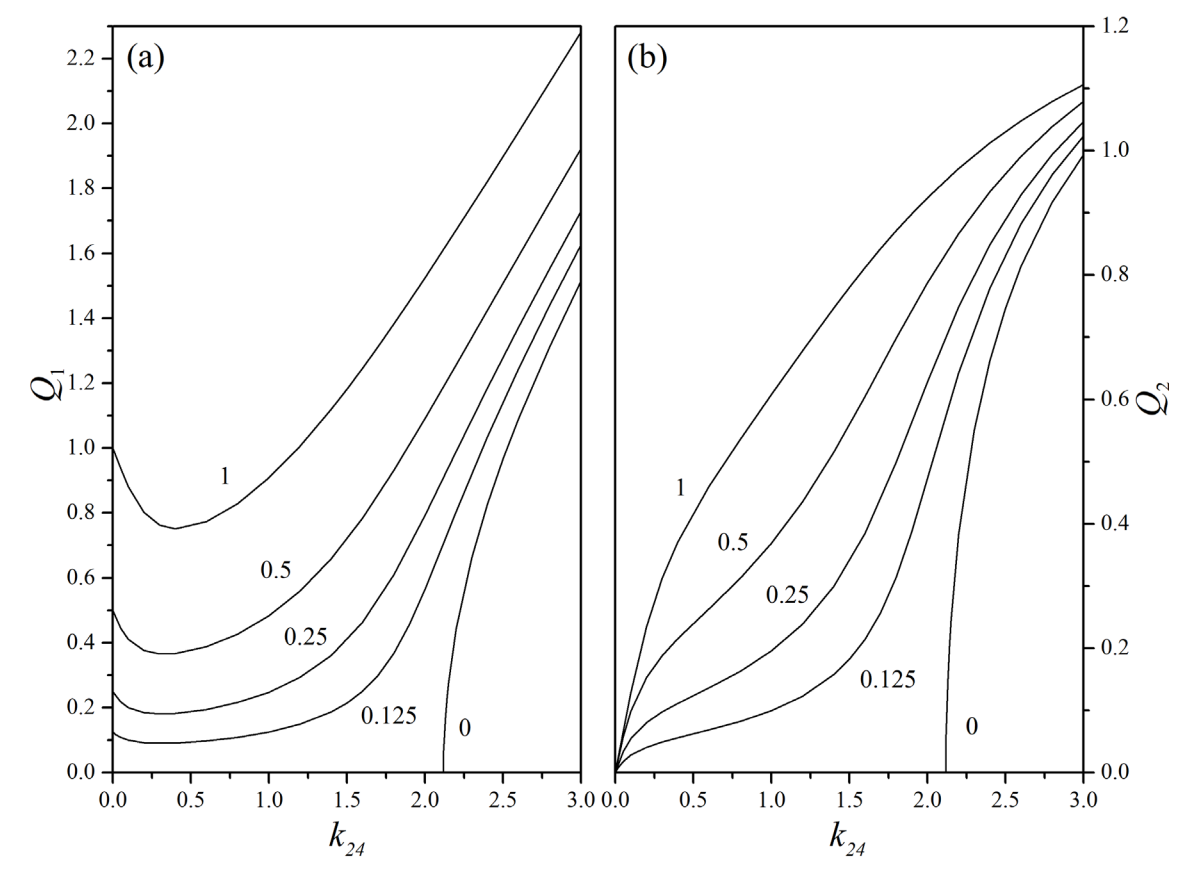


Figure 2. Dependence of *equilibrium* values of Q_1 (left) and Q_2 (right) on k_{24} for five different values of the intrinsic chirality Q (denoted by numbers in graphs). Homeotropic anchoring, w = 1.

2.3.2. RZT structure: tangential anchoring

For tangential anchorings the configurational variability of RZT structures is much more complex. This is illustrated in **Figure 3**, where we plot the dependencies of $Q_1(k_{24})$ and $Q_2(k_{24})$ on all studied anchoring conditions for two significantly different values of Q, viz., Q = 0.125 and Q = 1. The behavior is roughly similar for homeotropic and azimuthal anchoring, whereas for zenithal anchoring qualitatively different features emerge. In particular, Q_1 could even change sign at a critical value of k_{24} , which we denote by $k_{24}^{(c)}$. Similarly, for a given value of k_{24} this crossover could be achieved by varying Q, and we label the corresponding critical value by Q_c .

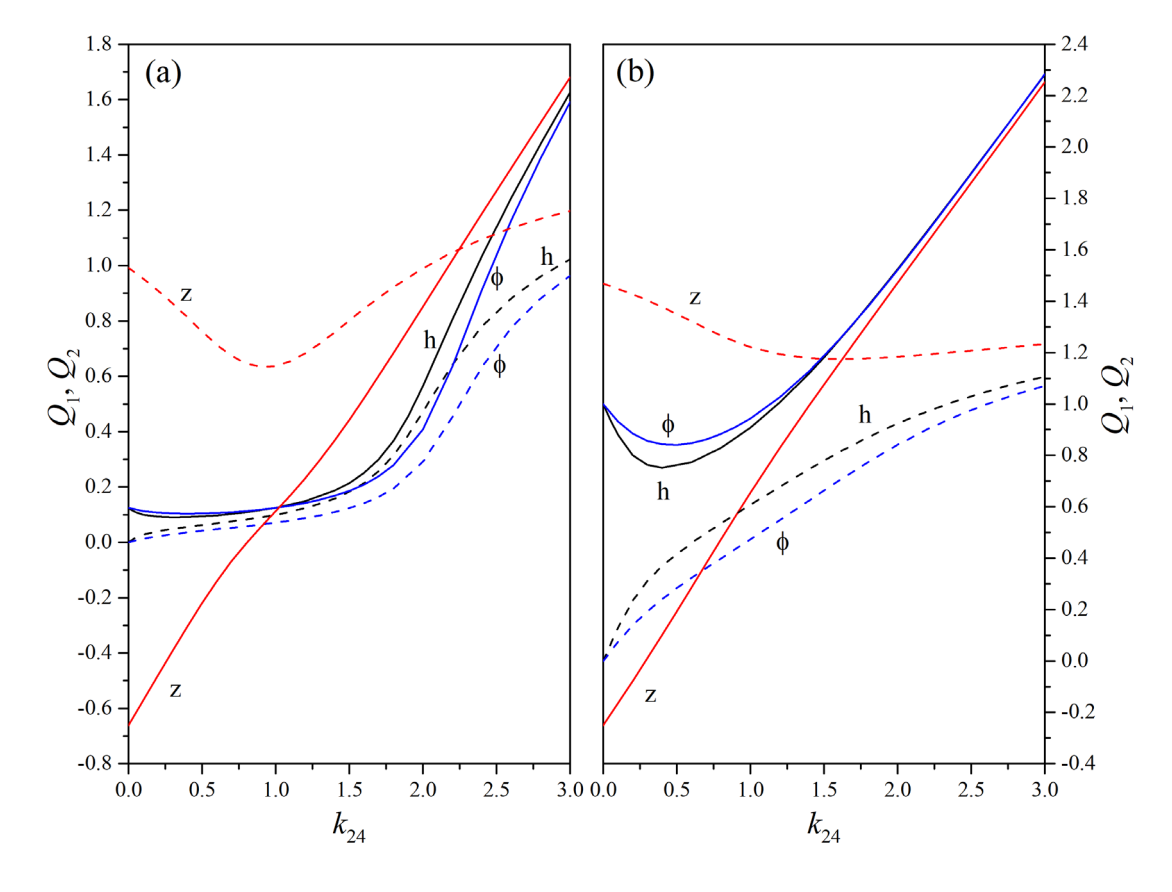
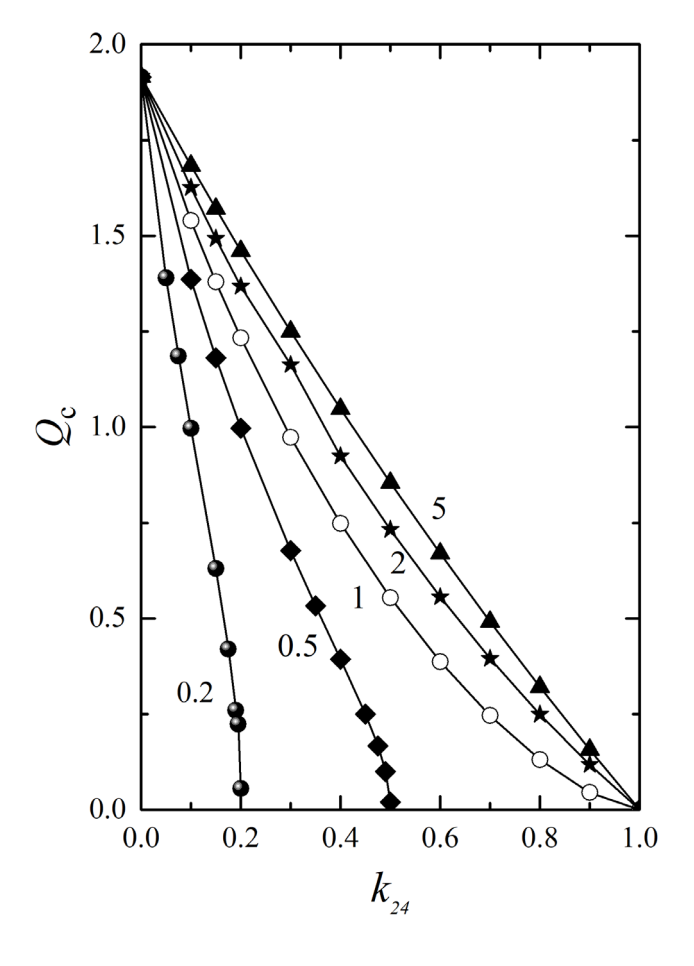


Figure 3. Dependence of Q_1 (solid lines) and Q_2 (dashed lines) on k_{24} for Q = 0.125 (left figure) and Q = 1 (right figure) and different types of anchoring, labelled by "h" (homeotropic), " ϕ " (azimuthal) and "z" (zenithal). w = 1.

Note that a value of $k_{24}^{(c)}$ depends relatively strongly on Q. Because the uniaxial twist with $Q_1 = 0$ can be observed easily by polarized optical microscopy, this phenomenon may be exploited to measure the splay–bend elastic constant. This is illustrated **Figure 4**, where we plot the $Q_c(k_{24})$ dependence for different anchoring strengths. Experimentally, one could vary Q by adding a chiral dopant to LC. The reversal of the sign of Q_1 exists in the interval $0 < k_{24} < 1$ well below $k_{24}^{(e)}$. In the strong anchoring limit $W \rightarrow \infty$ the graph $Q_c(k_{24})$ approaches the straight line.



260

261

262

263

264

265

266

267

268

269

270

271

272

273

274

275

276

277

278

279

280

281

Figure 4. The dependence of the critical intrinsic chirality Q_c (where $Q_1 = 0$) on k_{24} in the case of zenithal anchoring for different values of anchoring strength. Results were calculated in points labelled with symbols and lines serve as quides for the eye. From the left to right: w = 0.2 (circles), 0.5 (diamonds), 1 (open circles), 2 (stars) and 5 (triangles).

2.3.3. Relative stability of RZT and RT structures

The minimum energies (corresponding to local minima on varying variational parameters) of both types of structures (RZT and RT) were compared for different sets of parameters. In general, homeotropic anchoring favours RZT configurations. This is obvious since the nematic director of the RT structure is always parallel to the boundary plane at the cylinder boundary. On the other hand, for both types of tangential anchoring stability regimes of different structures depend on specific set of parameters k_{24} , Q and w. Due to a broad parameter space we limit our analysis to a few cases relevant for our study. For example, Figure 4 reveals the parameters for which $Q_1 = 0$ (chirality reversal) is realised for the RZT configuration for zenithal anchoring. It is essential to compare its free energy with the competitive RT structure. Some representative examples are depicted in Figure 5 and Figure 6. In Figure 5 we plot the minimum energies of the competing structures on varying Q for k24 = 0.5 and weak (w = 1) zenithal anchoring for the case exhibiting chirality reversal. In this case the RZT structure with $Q_1 < 0$ is metastable with respect to RT. However, **Figure 5** illustrates the existence of a regime for which the configuration with $Q_1 < 0$ is stable for k_{24} =0.25. Thus, chirality reversal may be found experimentally in this case. The arrows in Figure. 5 indicate approximately the energy of the RZT structure at the reversal of the sign of Q_1 , together with the calculated chirality parameters. For lower values of Q_i , it holds that $Q_1 < 0$, and vice versa. Although the energies for the cases $k_{24} =$ 0.25 and 0.5 are not very different, the critical value of Q ($Q_c = Q$, where Q_1 changes sign) differs significantly: $Q_c = 0.554$ for the case $k_{24} = 0.5$, whereas $Q_c = 1.097$ for the case $k_{24} = 0.25$.

283

284

285

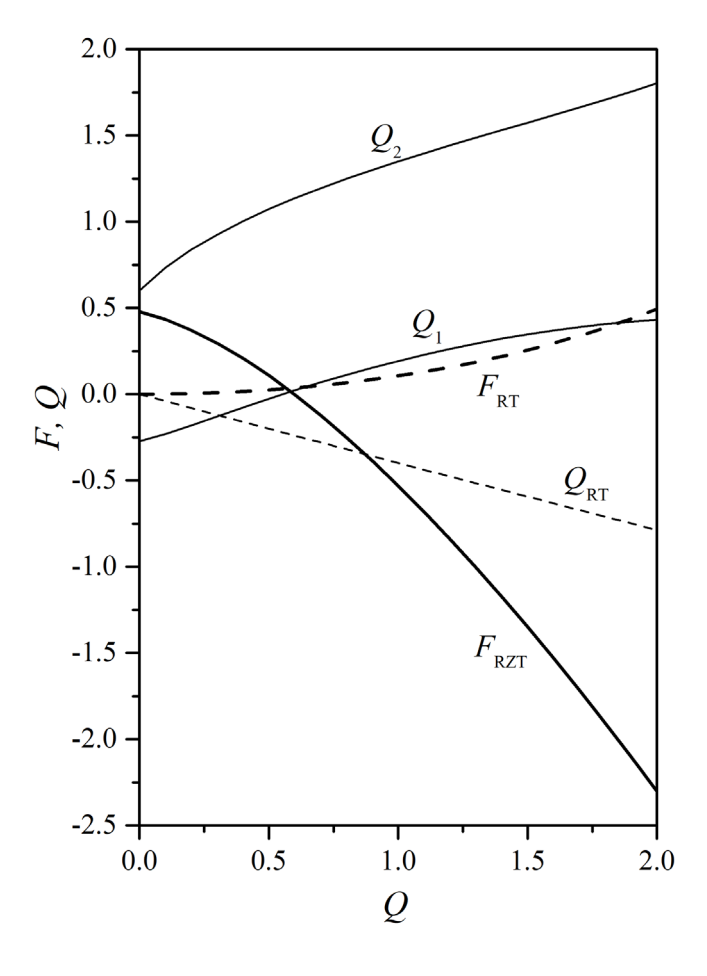


Figure 5. Dependence of the *minimum* energies (thick lines) and chirality parameters (thin lines) of the RZT structure (solid lines) and RT structure (dashed lines) on the intrinsic chirality Q. k_{24} = 0.5, zenithal anchoring with w = 1.

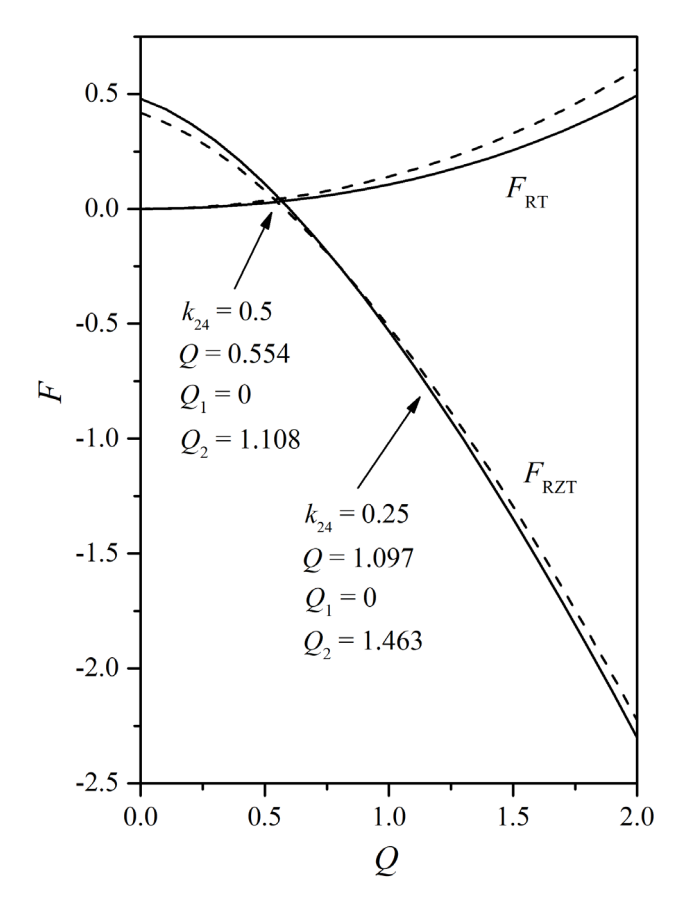


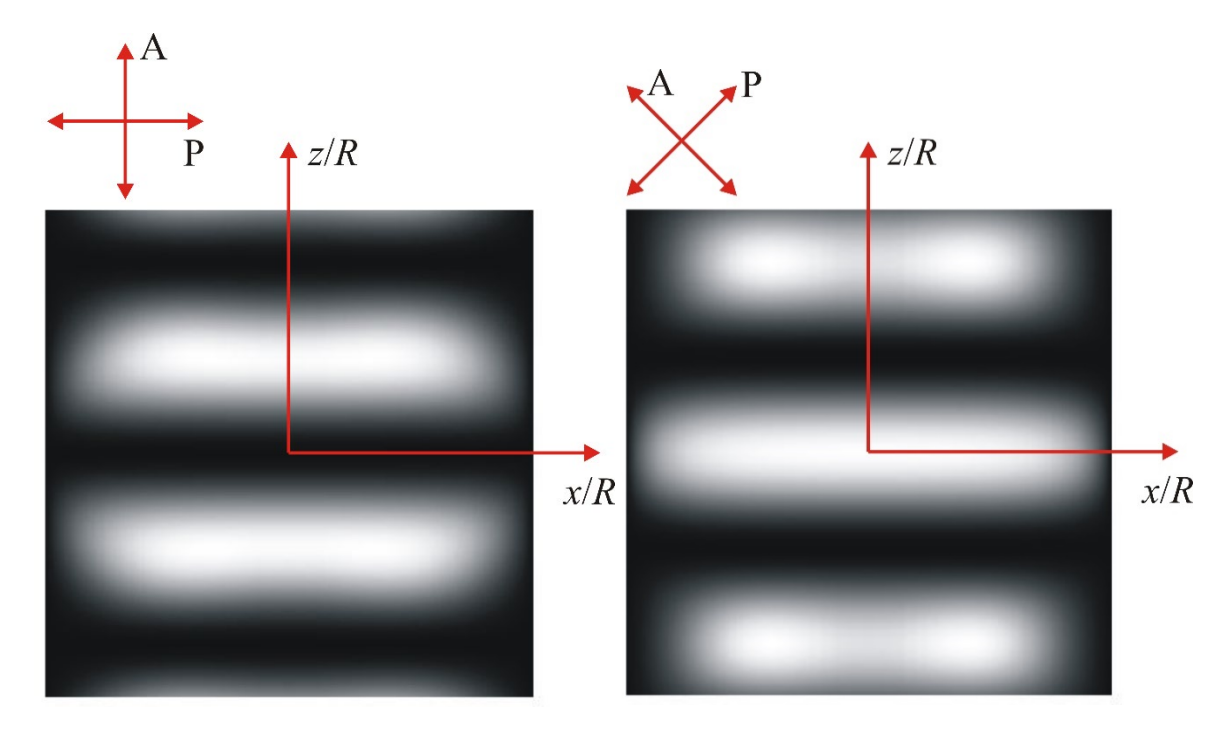
Figure 6. Dependence of the *minimum* energies of the RZT and RT structures on the intrinsic chirality Q. Solid lines: $k_{24} = 0.5$. Dashed lines: $k_{24} = 0.25$. Zenithal anchoring with w = 1. Arrows indicate the sign reversal of Q_1 for both values of k_{24} . For the case $k_{24} = 0.25$ the chirality Q_1 reverses sign in the regime where $F_{RZT} < F_{RT}$.

Note that we have tested the stability of RZT and RT structures with respect to the nonchiral escaped radial structure [34], in which the director profile exhibits cylindrical symmetry. It tends to be radially oriented at the cylinder wall and gradually reorients along the z axis on approaching the cylinder axis. For homeotropic anchoring, it exists for w = RW/K > 1, and its free energy is given by [34]

$$\frac{F}{\pi KH} = 3 - k_{24} - \frac{1}{\sigma'}$$

where $\sigma = w + k_{24} - 1$. In the region of our interest this structure is energetically costlier with respect to the competing RZT or RT structure.

Finally, in **Figure 7** and **Figure 8** we show calculated optical polarising microscopy patterns for the competing RZT and RT structures for two different polarisation directions of polariser and analyser, where we set $Q_1 = Q_2 = Q_{RT} = 1$. Simulations details are described in [29,30]. The polarisations of polariser and analyser are mutually perpendicular. The angle between the polariser and x-axis (horizontal axis) is 0 or 45°. One sees that the textures are significantly different and that one could easily distinguish these structures by using polarising optical microscopy.

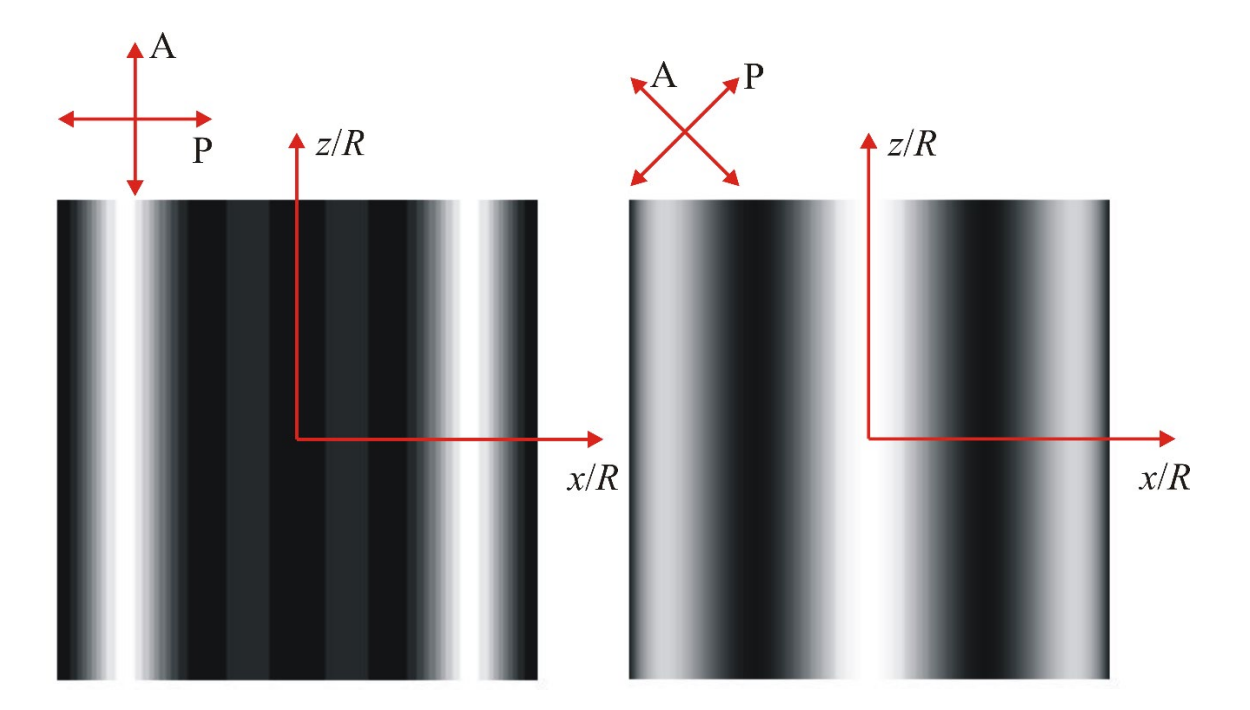


308

309

310

Figure 7. Calculated optical patterns for the RZT structure with $Q_1 = Q_2 = 1$. The transmitted polarisation of polariser is in the x-direction (left figure) and at the angle 45° with respect to x-direction (right figure). Optical data: $R = 1 \mu m$, laser light wavelength $\lambda = 445 nm$, refraction indices: $n_0 = 1.544$, $n_0 = 1.821$, corresponding to NLC E7.



311

312

313

Figure 8. The same as for **Figure 7**, but for RT structure with $Q_{RT} = 1$.

3. Conclusions

314315316317

We studied the impact of chirality, the saddle-splay elastic constant and anchoring conditions on the (meta) stability on radially-z-twisted (RZT), and radially-twisted (RT) configurations realised in a cylindrically confined confinement of radius *R*. We used the Frank-Oseen uniaxial description in terms of the nematic director field. Such a description is sensible because we do not consider

configurations exhibiting topological defects, which would require local melting of nematic order or the presence of biaxiality. Furthermore, we used the approximation of equal Frank elastic constants $K_{11} = K_{22} = K_{33} \equiv K$. We expressed the free energy of structures in terms of dimensionless wavenumbers Q_1 , Q_2 , Q_{RT} , which represent order parameters in our Landau-type analysis. The parameter space controlling the relative stability of the structures consists of the dimensionless chirality Q = Rq, dimensionless saddle-splay constant $k_{24} = K_{24}/K$, and dimensionless anchoring strength $w = \frac{RW}{K}$.

We found that in the absence of chirality the RZT structure could be (meta) stable (fulfilling the Ericksen's inequality $k_{24} < k_e \equiv 2$) only for isotropic tangential anchoring, provided that $k_{24} > 1 + \sqrt{1 - |w|/4}$. On the other hand, the RT structure could be (meta) stable for azimuthal anchoring condition and $k_{24} > 2 - |w|$. Yet chirality enables stability of RZT structures for k_{24} values in the interval $k_{24} \in [0,2]$. Furthermore, for $Q_{RT} < 1$ we found that the RT structures exhibit the wave vector $Q_{RT} \sim -Q/(2 + \Delta - k_{24})$, where i) $\Delta = 0$, ii) $\Delta = |w|$, iii) $\Delta = -|w|$ for i) homeotropic, ii) zenithal, and iii) azimuthal anchoring, respectively. In addition, we observed that the RZT configuration could exhibit sign reversal of the wave vector for zenithal anchoring on varying a relevant control parameter. This approach could be exploited for experimental determination of K_{24} values, which still require considerably more exploration.

Note that multiple-twisted structures could be exploited in several applications because their wave vectors can be adjusted to the optically visible regime. In 3D such structures could stabilise lattices of disclinations, as manifested in the Blue Phases and related structures exhibiting Skyrmion-like structures. The study of latter structures could also provide understanding into fundamental workings in nature which is still lacking.

4. Methods

325

326

327

328

329

330

331

332

333

334

335

336

337

338

339

340

341

342

351

We use the Frank-Oseen continuum approach [11] where nematic structures are expressed in terms of the nematic director field \vec{n} . The free energy of confined NLCs is expressed as

343
$$F = \iiint f_e d^3 \vec{r} + \iint f_s d^2 \vec{r}. \tag{17}$$

The first and second integral are carried over the LC volume and over a NLC confining surface.

The quantities f_e and f_s determine elastic and NLC-confining surface free energy density contributions.

347 The elastic term reads

348
$$f_e = \frac{\kappa_{11}}{2} (\nabla \cdot \vec{n})^2 + \frac{\kappa_{22}}{2} (\vec{n} \cdot \nabla \times \vec{n} + q)^2 + \frac{\kappa_{33}}{2} |\vec{n} \times \nabla \times \vec{n}|^2 - \frac{\kappa_{24}}{2} \nabla \cdot (\vec{n} \nabla \cdot \vec{n} + \vec{n} \times \nabla \times \vec{n}).$$
 (18)

The elastic response is determined by the splay (K_{11}) , twist (K_{22}) , bend (K_{33}) and saddle–splay (K_{24}) elastic constant, respectively. The wave vector q reflects the inherent LC chirality.

We model the surface interaction term using a simple Rapini-Papoular [11] description:

$$f_s = \frac{w}{2} (1 - (\vec{n}.\vec{e})^2). \tag{19}$$

Here the unit vector \vec{e} is commonly referred to as the easy axis. Namely, for W>0 the corresponding free energy is locally minimized if \vec{n} is aligned along \vec{e} . Furthermore, for W<0 the term is minimized for $\vec{n} \perp \vec{e}$.

Acknowledgments: A.G. acknowledges the support of AD FUTURA, Public Scholarship,
Development, Disability, and Maintenance Fund of the Republic of Slovenia. S.K. acknowledges the
support of a Slovenian Research Agency (ARRS) grant P1–0099. C.R. was supported by the National
Science Foundation Condensed Matter Physics program under grant DMR-1901797

- 360 Author contributions: A.M., S.K. and C.R. proposed and guided the research. A.M. did numerical
- simulations, A.G. did analytical analysis. A.M. and F.A. prepared figures. All authors were involved
- in writing the paper.

Supplementary files: Twisted nematic structures







Qrt.mp4

364

363

- Q₁Q₂ movie shows the radially-z-twist deformation and here the twist is realised both along the \vec{e}_{φ}
- and \vec{e}_z directions. The values were used in the movie from $Q_1 = 0.0$ to 3.0, and $Q_2 = 0.0$ to 3.0.
- Similarly, Qrt movie shows the radially twisted structure, and here the twist is realised along \vec{e}_r . The
- values were used in the movie from $Q_{RT} = 0.0$ to 3.0.

369 Abbreviations

370 The following abbreviations are used in this manuscript:

LC: liquid crystal BP: blue phase

RZT: radially-z-twisted RT: radially twisted

NLC: nematic liquid crystal

371 References

- 1. Pasteur, L. Memoires sur la relation qui peut exister entre la forme crystalline et al composition chimique, et sur la cause de la polarization rotatoire. *Compt. rend.* **1848**, *26*, 535–538.
- Harris, A.B.; Kamien, R.D.; Lubensky, T.C. Molecular chirality and chiral parameters. *Rev. Mod. Phys.* **1999**, *71*, 1745–1757.
- 376 3. Green, M.M.; Jain, V. Homochirality in Life: Two Equal Runners, One Tripped. *Orig. Life Evol. Biospheres* 2010, 40, 111–118.
- 4. Li, H.; Xu, S.; Rao, Z.-C.; Zhou, L.-Q.; Wang, Z.-J.; Zhou, S.-M.; Tian, S.-J.; Gao, S.-Y.; Li, J.-J.; Huang, Y.-B. Chiral fermion reversal in chiral crystals. *Nat. Commun.* **2019**, *10*, 1–7.
- 5. Green, M.M.; Peterson, N.C.; Sato, T.; Teramoto, A.; Cook, R.; Lifson, S. A Helical Polymer with a Cooperative Response to Chiral Information. *Science* **1995**, *268*, 1860–1866.
- Hendry, E.; Carpy, T.; Johnston, J.; Popland, M.; Mikhaylovskiy, R.V.; Lapthorn, A.J.; Kelly, S.M.; Barron,
 L.D.; Gadegaard, N.; Kadodwala, M. Ultrasensitive detection and characterization of biomolecules using
 superchiral fields. *Nat. Nanotechnol.* 2010, 5, 783–787.
- 7. Soukoulis, C.M.; Wegener, M. Past achievements and future challenges in the development of threedimensional photonic metamaterials. *Nat. Photonics* **2011**, *5*, 523–530.
- 387 8. Zhang, S.; Park, Y.-S.; Li, J.; Lu, X.; Zhang, W.; Zhang, X. Negative Refractive Index in Chiral Metamaterials. *Phys. Rev. Lett.* **2009**, *102*, 023901.
- 9. Wu, L.; Sun, H. Manipulation of cholesteric liquid crystal phase behavior and molecular assembly by molecular chirality. *Phys. Rev. E* **2019**, *100*, 022703.
- 391 10. Kim, Y.; Yeom, B.; Arteaga, O.; Jo Yoo, S.; Lee, S.-G.; Kim, J.-G.; Kotov, N.A. Reconfigurable chiroptical nanocomposites with chirality transfer from the macro- to the nanoscale. *Nat. Mater.* **2016**, *15*, 461–468.
- 393 11. Kleman, M.; Laverntovich, O.D. *Soft Matter Physics: An Introduction*; Springer Science & Business Media: New York, 2007; ISBN 0387952675.

- 395 12. Palffy-Muhoray, P. The diverse world of liquid crystals. *Physics Today* **2007**, *60*, 54–60.
- 396 13. Sparavigna, A.; Lavrentovich, O.D.; Strigazzi, A. Periodic stripe domains and hybrid-alignment regime in nematic liquid crystals: Threshold analysis. *Phys. Rev. E* **1994**, *49*, 1344–1352.
- 398 14. Lavrentovich, O.D.; Pergamenshchik, V.M. Patterns in thin liquid crystals films and the divergence ("surfacelike") elasticity. *Int. J. Mod. Phys. B* **1995**, *09*, 2389–2437.
- 400 15. Ericksen, J.L. Inequalities in Liquid Crystal Theory. *Phys. Fluids* **1966**, *9*, 1205–1207.
- 401 16. Polak, R.D.; Crawford, G.P.; Kostival, B.C.; Doane, J.W.; Žumer, S. Optical determination of the saddle-splay elastic constant K24 in nematic liquid crystals. *Phys. Rev. E* **1994**, *49*, R978–R981.
- 403 17. Allender, D.W.; Crawford, G.P.; Doane, J.W. Determination of the liquid-crystal surface elastic constant K24. *Phys. Rev. Lett.* **1991**, *67*, 1442–1445.
- 405 18. Crawford, G.P.; Allender, D.W.; Doane, J.W. Surface elastic and molecular-anchoring properties of nematic liquid crystals confined to cylindrical cavities. *Phys. Rev. A* **1992**, *45*, 8693–8708.
- 407 19. Selinger, J.V. Interpretation of saddle-splay and the Oseen-Frank free energy in liquid crystals. *Liq. Cryst.* 408 *Rev.* **2018**, *6*, 129–142.
- 409 20. Mermin, N.D. The topological theory of defects in ordered media. *Rev. Mod. Phys.* **1979**, *51*, 591–648.
- 410 21. Kurik, M.V.; Lavrentovich, O.D. Defects in liquid crystals: homotopy theory and experimental studies. 411 *Sov. Phys. Usp.* **1988**, *31*, 196–224.
- 412 22. Meiboom, S.; Sammon, M. Structure of the Blue Phase of a Cholesteric Liquid Crystal. *Phys. Rev. Lett.*413 1980, 44, 882–885.
- 414 23. Ravnik, M.; Alexander, G.P.; Yeomans, J.M.; Zumer, S. Three-dimensional colloidal crystals in liquid crystalline blue phases. *Proc. Natl. Acad. Sci.* **2011**, *108*, 5188–5192.
- 416 24. Jo, S.-Y.; Jeon, S.-W.; Kim, B.-C.; Bae, J.-H.; Araoka, F.; Choi, S.-W. Polymer Stabilization of Liquid-417 Crystal Blue Phase II toward Photonic Crystals. *ACS Appl. Mater. Interfaces* **2017**, *9*, 8941–8947.
- 418 25. Schopohl, N.; Sluckin, T.J. Defect Core Structure in Nematic Liquid Crystals. *Phys. Rev. Lett.* **1987**, *59*, 419 2582–2584.
- 420 26. Ambrožič, M.; Žumer, S. Chiral nematic liquid crystals in cylindrical cavities. *Phys. Rev. E* **1996**, *54*, 5187–421 5197.
- 422 27. Ambrožič, M.; Žumer, S. Axially twisted chiral nematic structures in cylindrical cavities. *Phys. Rev. E* 423 1999, *59*, 4153–4160.
- 424 28. Jeong, J.; Kang, L.; Davidson, Z.S.; Collings, P.J.; Lubensky, T.C.; Yodh, A.G. Chiral structures from achiral liquid crystals in cylindrical capillaries. *Proc. Natl. Acad. Sci.* **2015**, *112*, E1837–E1844.
- 426 29. Crawford, G.P.; Mitcheltree, J.A.; Boyko, E.P.; Fritz, W.; Zumer, S.; Doane, J.W. K33/K11 determination in nematic liquid crystals: An optical birefringence technique. *Appl. Phys. Lett.* **1992**, *60*, 3226–3228.
- 30. Polak, R.D.; Crawford, G.P.; Kostival, B.C.; Doane, J.W.; Žumer, S. Optical determination of the saddle-splay elastic constant K 24 in nematic liquid crystals. *Phys. Rev. E* **1994**, 49, R978–R981.
- 430 31. Ondris-Crawford, R.J.; Ambrožič, M.; Doane, J.W.; Žumer, S. Pitch-induced transition of chiral nematic liquid crystals in submicrometer cylindrical cavities. *Phys. Rev. E* **1994**, *50*, 4773–4779.
- 432 32. Hobson, A. There are no particles, there are only fields. *Am. J. Phys* **2013**, *81*, 211–223.
- 433 33. Skyrme, T.H.R. A unified field theory of mesons and baryons. *Nucl. Phys.* **1962**, *31*, 556–569.
- 34. Crawford, G.P.; Allender, D.W.; Doane, J.W. Surface elastic and molecular-anchoring properties of nematic liquid crystals confined to cylindrical cavities. *Phys. Rev. A* **1992**, *45*, 8693–8708.



© 2020 by the authors. Submitted for possible open access publication under the terms and conditions of the Creative Commons Attribution (CC BY) license (http://creativecommons.org/licenses/by/4.0/).